Dalton Transactions

PAPER

View Article Online
View Journal | View Issue

Cite this: *Dalton Trans.*, 2014, **43**, 12982

Au nanoparticles in carbon nanotubes with high photocatalytic activity for hydrocarbon selective oxidation†

Juan Liu, Ruihua Liu, Haitao Li, Weiqian Kong, Hui Huang, Yang Liu* and Zhenhui Kang*

Received 11th April 2014,
Accepted 4th July 2014

DOI: 10.1039/c4dt01077a

www.rsc.org/dalton

High-efficiency and high-selectivity catalytic oxidation of alkanes under mild conditions with air is a major aim of current catalytic chemistry and chemical production. Despite extensive development efforts on new catalysts for cyclohexane oxidation, current commercial processes still suffer from low conversion, poor selectivity, and excessive production of waste. Here, we present the design and synthesis of gold nanoparticle/carbon nanotube (CNT) composites for high-efficiency and high-selectivity photocatalyst systems for the green oxidation of cyclohexane. Remarkably, Au nanoparticles confined in carbon nanotubes (Au-in-CNTs) are photocatalytically active for the oxidation of cyclohexane with 14.64% conversion of cyclohexane and a high selectivity of 86.88% of cyclohexanol using air and visible light at room temperature. Given its diversity and versatility of structural and composition design, gold nanoparticle/CNT composites may provide a powerful pathway for the development of high-performance catalysts and production processes for green chemical industry.

Introduction

Catalyzing partial oxidation of small hydrocarbons using molecular oxygen has been a very important process used to obtain industrially important chemicals.[1,2] The present commercial process for cyclohexane oxidation is carried out at around 423 K and 1–2 MPa pressure, affording ~4% conversion and ~60% selectivity to cyclohexanone and cyclohexanol over metal cobalt salt or metal-boric acid. Although many efforts have been made to develop new catalysts (such as iron-based catalyst systems,[3–5] cobalt or manganese salts,[6] copper species within SBA-15,[7] Fe_2O_3–TiO_2,[8] and Al-HMS[9]) to oxidize cyclohexane under mild conditions, the present commercially-practiced process suffers from low yields (<8%), poor selectivity (<50%), as well as production of greenhouse gases and large quantities of waste. So oxidizing cyclohexane with high conversion and high selectivity under mild conditions is still a great challenge for experimental study.

Institute of Functional Nano & Soft Materials (FUNSOM), Jiangsu Key Laboratory for Carbon-based Functional Materials and Devices, and Collaborative Innovation Center of Suzhou Nano Science and Technology, Soochow University, Suzhou, Jiangsu, China. E-mail: yangl@suda.edu.cn, zhkang@suda.edu.cn

†Electronic supplementary information (ESI) available: Details of experiment description, HRTEM images of short CNTs, ESR spectra of the DMPO-˙OH (aqueous solution) adducts for the Au-in-CNT-H_2O_2 system, RRDE voltammograms of Au-in-CNTs (Au-out-CNTs) and calculation of the H_2O_2 yield. See DOI: 10.1039/c4dt01077a

Noble metal nanoparticles (NPs) (*i.e.* Ag, Au) can strongly absorb visible light due to their surface plasmon resonance (SPR, it can be tuned by varying their size, shape and surrounding), working as an electron trap and active reaction site, which gave rise to a new approach to efficient visible light photocatalysts.[10–15] In general, the visible-light plasmonic photocatalyst is a composite photocatalyst composed of noble-metal NPs and a polar semiconductor, but recently other materials such as carbon,[16] graphene oxide, graphene, and oxide insulators have also been used as supports and/or charge carriers to form plasmonic photocatalysts. On the other hand, carbon nanotubes (CNTs) with high electron and thermal conductivity, high surface area, and functionalizable surfaces have evoked wide interest for catalytic applications.[17–23] As a catalyst additive, CNTs promoted substantially the catalytic activities of catalysts. Particularly, their channels are anticipated to provide an intriguing confinement environment for metal catalysts and catalytic reactions, which may provide opportunities for the development of new heterogeneous catalysts.[24–28] Many researchers reported that metal catalysts introduced into the CNT channels were essential to achieve the optimized catalytic activity.[29–33] This opens up an opportunity to tune the catalytic performance *via* confinement inside CNTs. Although metal catalysts confined in CNTs were studied for many years, fewer reports focused on the light-induced catalysis process based on this type of catalyst. Considering the intriguing confinement environment of CNT

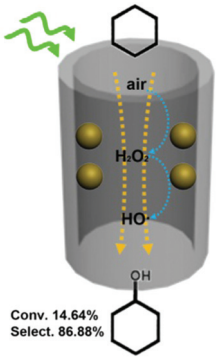

Scheme 1 Au-in-CNTs composites as photocatalysts for selective oxidation of cyclohexane using air as the oxidant under visible light.

channels and the SPR effect of metal NPs, the combination of CNTs and metal NPs may be regarded as an ideal strategy to construct the stable and efficient complex for high efficiency oxidation of cyclohexane under visible light.

Herein, we present the design and synthesis of Au NP/CNT composites for high-efficiency and high-selectivity photocatalyst systems for the green oxidation of cyclohexane. In the present catalyst system, Au nanoparticles were confined in CNTs (Au-in-CNTs), which are photocatalytically active, and can lead to the oxidation of cyclohexane with 14.64% conversion of cyclohexane and a high selectivity of 86.88% of cyclohexanol using air and visible light at 333 K (see Scheme 1). A series of catalytic experiments suggested that the high conversion and selectivity in the present photocatalyst system should be attributed to the collective contribution of Au NPs and the confinement reaction space in CNTs.

Results and discussion

Characterization of Au-in-CNT composites

In our experiment, the raw CNTs were treated with concentrated sulfuric and nitric acids, and the obtained products were short-CNTs with open ends (see Fig. S1 in the ESI†). Au-in-CNT composites were fabricated by addition of the short-CNTs to $HAuCl_4$ solution with vigorous magnetic stirring in the dark at room temperature (see the Experimental section for details). The transmission electron microscopy (TEM) image of Au-in-CNTs (Fig. 1a) shows that the Au nanoparticles with a size of about 3.6 nm (for the size distribution see Fig. 1b) are evenly distributed within the CNT channels. Fig. 1a inset pattern presents the high resolution TEM (HRTEM) image of Au-in-CNTs. The encapsulated Au nanoparticles and carbon nanotubes exhibit typical lattice fringes with *d*-spacings of 0.23 and 0.34 nm, in well agreement with the (111) planes of crystalline Au and (002) crystallographic planes of graphitic carbon respectively. Fig. 1c shows the typical Raman scattering peaks of CNTs at 1329.5, 1578.2 and 2644.7 cm^{-1},[34] in which the Raman signal intensity is enhanced by Au nanoparticles owing to their surface enhancement Raman scattering effects.[35] Among the above three

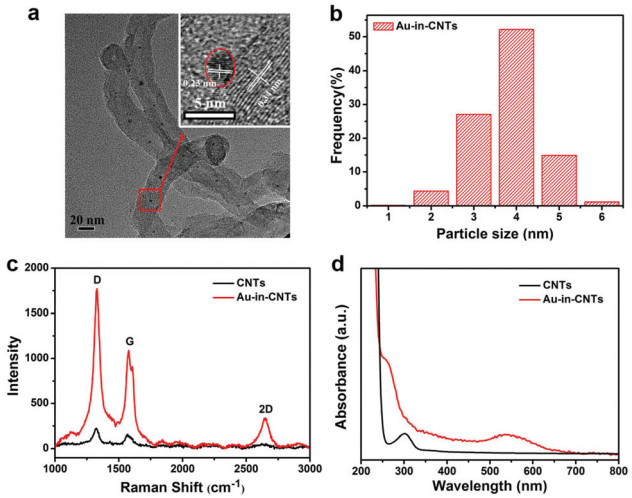

Fig. 1 (a) TEM image, high resolution TEM (HRTEM) pattern (inset) of Au-in-CNTs; (b) Au nanoparticle size distribution is based on TEM characterization shown in (a); (c) typical Raman spectra of CNTs (black trace) and Au-in-CNTs (red trace); (d) the UV-Vis absorbance spectrum of CNTs (black trace) and Au-in-CNTs (red trace).

Raman scattering peaks, the former two strong peaks correspond to the first-order D and G bands of CNTs. Here, the G band splits into two peaks, in which the peaks centered at 1578.2 and 1606.8 cm^{-1} correspond to G^- and G^+ bands, respectively. These two splitting peaks contribute to E_{2g} mode of graphite of metallic ≠ semiconducting type.[36] The D-band peak is attributed to the emergence of the crystallite size effect, which makes some of the non Raman-active phonons active.[37] The two-order D peak (at 2644.7 cm^{-1}) is also obviously turned up when Au nanoparticles are confined in CNTs. Fig. 1d shows UV-vis absorption spectra recorded of the solid powder corresponding to the sample shown in Fig. 1a. The bare CNTs exhibit an obvious sharper peak centered at around 300 nm which derives from the C=C structure of mixed acid treated CNTs.[38] Compared with that of CNTs, the UV-Visible absorption spectrum of Au-in-CNTs displays typical absorbance in both UV (at 262 nm) and visible regions (at 538 nm). Typically, Au particles of about 5 nm show one major plasmon absorption peak at 510–520 nm. However, here, the Au plasma band red shifted to a longer wavelength with a broad peak exhibited at about 538 nm, while the CNT absorption band blue shifted to a shorter wavelength. This phenomenon probably is attributed to the electron transferred from Au to connected CNTs.[39,40]

Catalytic oxidation of cyclohexane using Au-in-CNT composites

The catalytic activity of the synthesized Au-in-CNTs is tested by the oxidation reaction of cyclohexane. In detail, the mixture of Au-in-CNTs composites (50 mg), cyclohexane (10 mL) and *tert*-butyl hydroperoxide (TBHP, 0.5 mL, is used as a radical initiator) are mixed together in a round bottom flask (250 mL) with water condenser and continuous magnetic stirring at

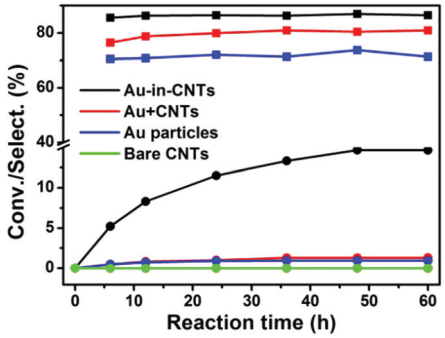

Fig. 2 Time dependence of the conversion and selectivity of the oxidation of cyclohexane with different materials as photocatalysts under Xe lamp irradiation in the dark.

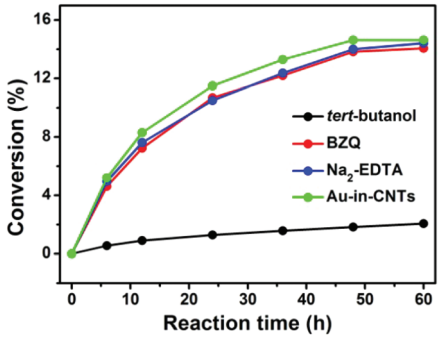

Fig. 3 Photocatalytic activities of Au-in-CNTs in reactive species trapping experiments with three kinds of reactive species scavengers.

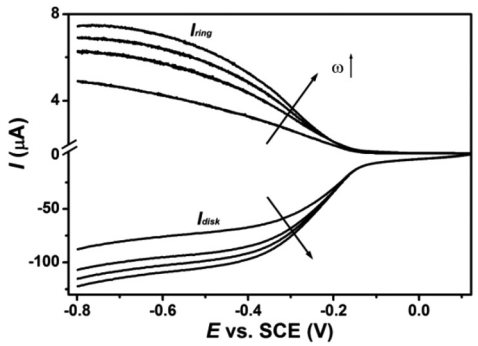

Fig. 4 Steady state voltammograms for the ORR, in air-saturated 0.1 M KOH, at Pt disk (modified with Au-in-CNT)-Pt ring electrodes (RRDE) at rotation rates of 100, 400, 900, 1600 rpm (from inner to outer). The Pt ring was polarized at +0.5 V *vs.* SCE. Potential scan rate of the disk electrode: 20 mV s^{-1}.

333 K, air as the oxidant. The oxidation products were analysed by gas chromatography (GC). Fig. 2 shows the time dependence of the conversion and selectivity of cyclohexane oxidation to cyclohexanol with Au-in-CNTs as the photocatalyst driven by visible light. It reveals that the conversion efficiency increases with increasing reaction time, while the selectivity to cyclohexanone is nearly constant at 86.9%. After 48 h reaction, a high conversion efficiency of 14.7% and a high selectivity of over 86.88% were achieved concurrently.

In general, HO$^{\bullet}$ is a strong oxidant, and can easily oxidize cyclohexane to cyclohexanone and cyclohexanol. A spin-trapping electron spin resonance (ESR) test was carried out to check the active oxygen species produced by the Au-in-CNT-water system under visible light. As shown in Fig. S2,† typical characteristic quartet peaks of the DMPO-$^{\bullet}$OH (DMPO, dimethyl pyridine *N*-oxide) adduct appeared gradually upon light irradiation of the aqueous Au-in-CNT-water system, which suggested that HO$^{\bullet}$ is the active oxygen species in this photocatalytic oxidation process. For further confirming this point, reactive species trapping experiments are carried out to investigate the reactive oxygen species in the photocatalytic oxidation process.[41] In this part, three different scavengers, *tert*-butanol (a $^{\bullet}$OH radical scavenger), BZQ (a $O^{2-\bullet}$ radical scavenger) and disodium ethylenediaminetetraacetate (Na_2-EDTA, a hole scavenger), are used. The photocatalytic performances in Fig. 3 show that the addition of *tert*-butanol substantially reduced the photocatalytic activity for the oxidation of cyclohexane from almost 15% to 2% in 60 h. The introduction of BZQ and Na_2-EDTA does not affect the photocatalysis results. It implies that a $^{\bullet}$OH radical is the main reactive species, while $O^{2-\bullet}$ radicals and holes do not contribute to the photocatalytic performance. The addition of *tert*-butanol traps the $^{\bullet}$OH radicals leading to low conversion of cyclohexane. It confirms that in the buffer solution containing the Au-in-CNT catalyst, a larger number of HO$^{\bullet}$ will be produced with visible light irradiation.

To further confirm the HO$^{\bullet}$ evolution, a series of electrochemical measurements (with the rotating ring disk electrodes (RRDE)) were carried out.[42] Fig. 4 shows the steady-state hydrodynamic voltammograms (RRDE) for the ORR at the Au-in-CNT modified Pt disk in air-saturated 0.1 M KOH at different rotation speeds. The top curves of each plot represent the corresponding Pt ring current (IR) of the relevant disk electrode (due to the oxidation of HO_2^- generated at the disk electrode). The Pt ring is potentiostated at 0.5 V. Obviously, the Pt ring current (I_{ring}) is clearly observed, indicating the contribution of the 2-electron reduction mechanism in the ORR. The H_2O_2 yield (%) is 40.38%, calculated using eqn (1) in ESI.†

Subsequently, the electrocatalytic ability of Au-in-CNTs modified GC electrodes toward H_2O_2 decomposition is analysed in a conventional three-electrode electrochemical cell with Au-in-CNTs modified GC electrodes as the working electrode, platinum wire as the counter electrode, and Ag/AgCl (saturated KCl) as the reference electrode. Fig. 5 shows the cyclic voltammograms of Au-in-CNTs modified GC electrodes in 0.05 M (pH = 7.4) phosphate buffer in the presence of different concentrations (0, 0.01 and 0.05 M) of H_2O_2 respectively. It is obviously shown that the reduction in current intensity of H_2O_2 at −0.80 V on Au-in-CNTs modified GC electrodes becomes much larger when increasing the H_2O_2 concentration. This phenomenon indicates that Au-in-CNTs modified GC electrodes possess an excellent catalytic ability toward the H_2O_2 decomposition. Thus, in the present system, the generation of HO$^{\bullet}$ can be concluded in Scheme 2. First, O_2 in air is partly catalytically reduced to H_2O_2 by Au-in-CNTs under light

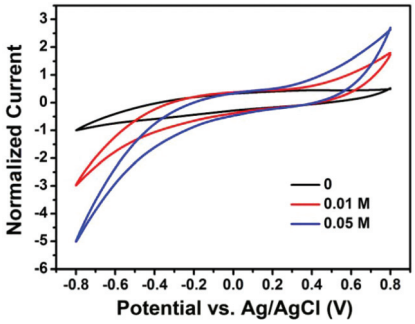

Fig. 5 Cyclic voltammograms of Au-in-CNTs modified GC electrodes in 0.05 M (pH = 7.4) phosphate buffer in the presence of different concentrations of H_2O_2 at a scan rate of 50 mV s^{-1}.

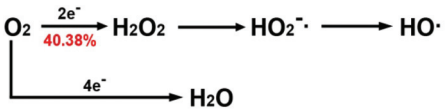

Scheme 2 Schematic illustration of the possible pathways of hydroxyl radical generation.

irradiation *via* a 2-electron ORR process. Then the $HO_2^{-\bullet}$ decomposes to free HO$^\bullet$, which is more stable and more active than the initial H_2O_2.

SECM measurements of Au-in-CNTs composites

Printed Au-in-CNTs spots are prepared as described in the Experimental section. The ultramicroelectrode (UME) was first positioned at about 15 μm from the substrate surface using approach curves in $K_4Fe(CN)_6$ solution (4 mM). To begin with, lateral scans are performed over Au-in-CNTs spots in the *X*-axis direction as shown in Fig. 6. The mapping of these spots is then imaged in two dimensions. Comparing these two SECM curves (in Fig. 6), there is a significant increase in the measured current with light radiation (red trace) as the UME passing over the Au-in-CNTs spots, which indicate that as a result of their photoinduced current enhancement on the CNTs' surface. The present current enhancement of CNTs by light irradiation further confirmed that the internal Au NPs transferred electrons to their connected carbon nanotube walls. To further prove this point, the influences of light radiation over catalysts are detected using *I*–*t* curves. Both the catalysts were indeed able to generate significant photocurrent under irradiation (in Fig. S6†). In 0.1 M Na_2SO_4 solution, both Au-in/out-CNTs reveal photocurrent generation, but the photocurrent intensity of Au-in-CNTs is almost three fold more than that of Au-out-CNTs.

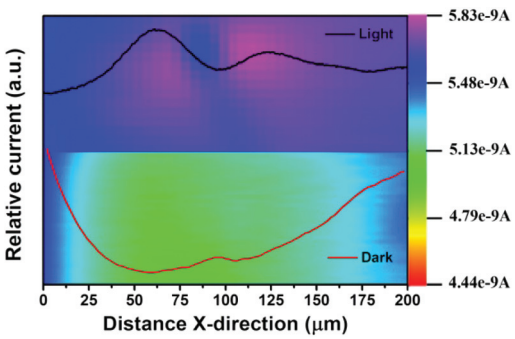

Fig. 6 SECM mapping and X-scan lines of Au-in-CNTs spots with light radiation (top part) and without light radiation (bottom part) scanned at a speed of 1 μm s^{-1}.

Surface plasmon resonance effect study

Cyclohexane oxidation was further carried out with the Au-in-CNTs composite catalyst driven by light of different wavelengths (Fig. 7). It shows that the best conversion efficiency is obtained under green light, whose wavelength matches the surface plasmon resonance zone of Au nanoparticles (500–600 nm).

Confinement effect study

For studying the confinement effect of carbon nanotubes, the Au nanoparticle loading on the outer wall of CNTs (Au-out-CNTs) is also prepared. The CNTs used in this experiment are untreated with the concentrated sulfuric and nitric acids. The location and particle size of Au are characterized by TEM analysis. The TEM image of Au-out-CNTs (Fig. 8a) clearly shows that the Au nanoparticles are dispersed on the outer wall surface of the CNTs. The average particle size of Au in Au-out-CNTs is about 4.5 nm, which are slightly larger than that of Au-in-CNTs. Fig. 8a inset pattern presents the HRTEM image of Au-out-CNTs with typical lattice fringes of (002) crystallographic planes of graphitic carbon and (111) planes of crystalline Au respectively. In Fig. 8c, the Raman signals of CNTs are also enhanced by the loaded Au nanoparticles. Fig. 8d shows UV-Vis absorption spectra obtained of the solid powder corresponding to the sample shown in Fig. 8a. For Au-out-CNTs, the absorption peak at about 300 nm corresponding to bare CNTs slightly blue shifts to 287 nm. In the visible light range, a broad peak exhibited at 500–700 nm, which is the result of surface plasmon resonance of different sizes of Au nanoparticles.

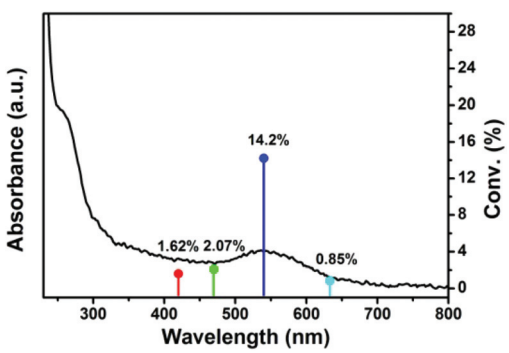

Fig. 7 Excitation wavelength dependence of the conversion of the oxidation of cyclohexane with Au-in-CNTs composites as photocatalysts by different lighting conditions: blue (420 nm), blue-green (470 nm), green (540 nm), and red (633 nm), using high power (>1 W) LED as the light source.

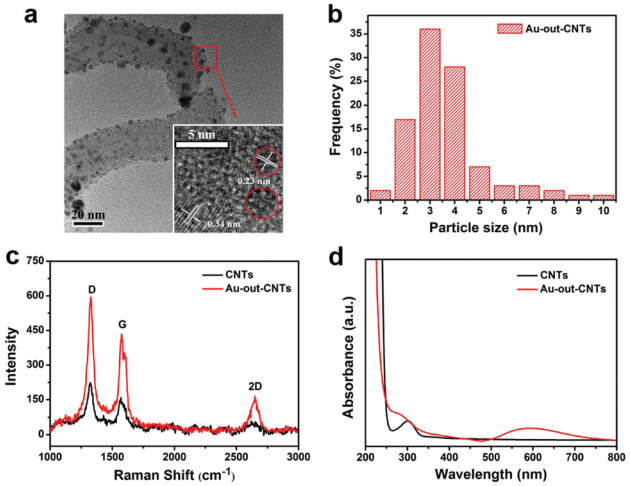

Fig. 8 (a) TEM image, high resolution TEM (HRTEM) pattern (inset) of Au-out-CNTs; (b) Au nanoparticle size distribution is based on TEM characterization shown in (a); (c) typical Raman spectra of CNTs (black trace) and Au-out-CNTs (red trace); (d) the UV-Vis absorbance spectrum of CNTs (black trace) and Au-in-CNTs (red trace).

In the following catalytic experiments, a mixture of Au-out-CNTs composites (50 mg), cyclohexane (10 mL) and TBHP (0.5 mL) was treated in a round bottom flask (250 mL) using air as the oxidant and a water condenser under continuous magnetic stirring at 333 K. The oxidation products were analyzed by gas chromatography (GC). Fig. 9 shows the time dependence of the conversion and selectivity of cyclohexane oxidation to cyclohexanol with Au-out-CNTs as the photocatalyst driven by visible light. It reveals that the conversion efficiency increases with increasing reaction time, while the selectivity to cyclohexanone is about 70.28%. After 48 h reaction, a conversion efficiency of 3.45% is achieved which is much lower than that of Au-in-CNTs.

Proposed mechanism study

For further studying the proposed mechanism, a series of control experiments are carried out. Table 1 lists the catalytic performances of different catalysts. The contrast of Au-in-CNTs (entry 2) and Au-out-CNTs (entry 3) indicates that Au nanoparticles confined in CNTs have a significant impact on the catalytic behavior. The conversion of cyclohexane at 48 h was elevated from 3.45 to 14.64%, corresponding to a fourfold increase when Au nanoparticles were confined in CNTs. Meanwhile, the cyclohexanol (Cy-OH) selectivity of Au-in-CNTs reaches 86.88%, indicating a promising selective production of cyclohexanol. Both catalysts show higher conversion than the pure Au catalyst (entry 1). In a word, CNTs as carriers play an important role in the selective catalysis oxidation process of cyclohexane. Light radiation is another factor for affecting the conversion and selectivity of Cy-OH (entry 4, control experiment b). Without Xe lamp emission, the conversion of cyclohexane with Au-in-CNTs is much lower than that under radiation, even lower than using Au-out-CNTs, which should be due to Au nanoparticles inside lacking the plasmon effect, and it is harder to contact with the reactant than outer Au nanoparticles. Under the conditions where the catalyst is not used, there is no Cy-OH or Cy=O found in the product (entry 5, control experiment c). There is also no target product obtained when TBHP is absent (entry 6, control experiment d).

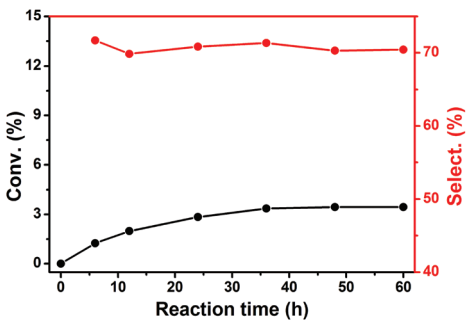

Fig. 9 Time dependence of the conversion (black line) and selectivity (red line) of the oxidation of cyclohexane with Au-out-CNTs as photocatalysts under Xe lamp irradiation.

Table 1 Conversion of cyclohexane and the cyclohexanol selectivity over different catalysts[a]

Entry	Catalyst [mg]	Au content [mg]	Conversion [%]	Selectivity [%] Cy=O	Cy-OH
Au NPs	0.05	0.05	0.94	9.29	80.39
Au-in-CNTs	50	0.05	14.64	12.79	86.88
Au-out-CNTs	50	0.05	3.45	5.94	70.28
Control[b]	50	0.05	2.65	13.56	62.99
Control[c]	50	0.05	3.16	31.25	47.01
Control[d]	0	0	0	0	0
Control[e]	50	0.05	0	0	0
Control[f]	50	0	0	0	0

[a] Reaction conditions: 333 K, in air, 48 h, with a Xe lamp, 10 ml cyclohexane, 50 mg catalyst, 0.5 ml *tert*-butyl hydroperoxide (TBHP). [b] Au-in-CNTs as the catalyst, without the Xe lamp. [c] Au-out-CNTs as the catalyst, without the Xe lamp. [d] Without any catalyst. [e] Without TBHP. [f] Bare CNTs.

In the following experiments, RRDE experiments were also performed with the Au-out-CNTs modified Pt disk electrode. As shown in Fig. 10, the Pt ring current (I_{ring}) is also clearly observed, indicating the contribution of the 2-electron reduction mechanism in the ORR. The H_2O_2 yield (%) of Au-out-CNTs catalysis ORR is 37.12%, which is smaller than Au-in-CNTs. A comparative inspection of the RRDE voltammograms in Fig. S3† reveals that the onset potential of the disk current flow corresponding to the ORR at the Au-in-CNTs modified electrode is positively shifted compared to the case of the Au-out-CNTs modified Pt disk.

Based on the above results and discussions, the proposed mechanism for the photoinduced catalytic ability of the present catalyst is described as follows. The surface plasmon resonance of Au NPs enhances the light absorption of Au-in-CNT composites. When Au NPs were assembled on CNTs (inside or outside), the excitation of the SPR of the Au NPs induced the charge transfer from the Au NPs to CNTs, which

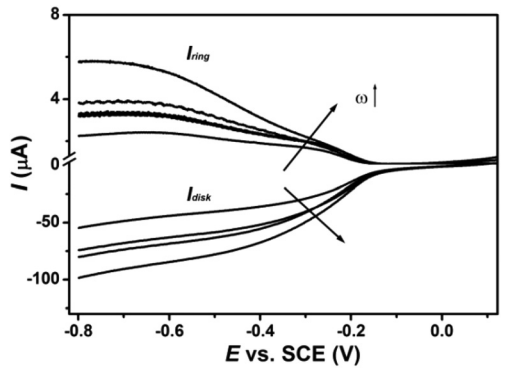

Fig. 10 Steady state voltammograms for the ORR, in air-saturated 0.1 M KOH, at Pt disk (modified with Au-in-CNTs)-Pt ring electrodes (RRDE) at rotation rates of 100, 400, 900, 1600 rpm (from inner to outer). The Pt ring was polarized at +0.5 V *vs.* SCE. Potential scan rate of the disk electrode: 20 mV s^{-1}.

enhanced the separation of photo-induced holes and electrons. At the interface of CNTs and Au NPs, O_2 was reduced to H_2O_2 and then decomposed into hydroxyl radicals ($HO^{\bullet}$) in the presence of an initiator (TBHP). $HO^{\bullet}$ serves as a strong oxidant for conversion of cyclohexane to cyclohexanone. In the process, the interaction between CNTs and Au NPs under visible light plays a key role in the eventual high conversion and selectivity. Confined Au nanoparticles proved surface plasmon resonance with Xe lamp irradiation, by which the active Au nanoparticles donate electrons to the attached internal CNT wall. For the space limitation of CNTs, the Au NP size in CNTs is smaller than Au NP loading on the outside wall. It is one reason for the higher catalytic activity of Au-in-CNTs. But the particle size is not the only factor that leads to the significant difference in the catalytic performance of the Au-in-CNTs and Au-out-CNTs catalysts. Besides that, confinement of reaction intermediates within such nanochannels might prolong their contact time with the catalyst as reported in the literature.[43]

To evaluate the stability of the catalyst, the recycling of Au-in-CNTs is performed for the catalyzed oxidation of cyclohexane (as shown in Fig. 11). The catalyst is recovered by centrifugation, washed with ethanol and water, and dried at 323 K in air. The average conversion rate of 14.525 and the selectivity of Cy-OH of 87.660 are very close to the original result (entry 7, control experiment f).

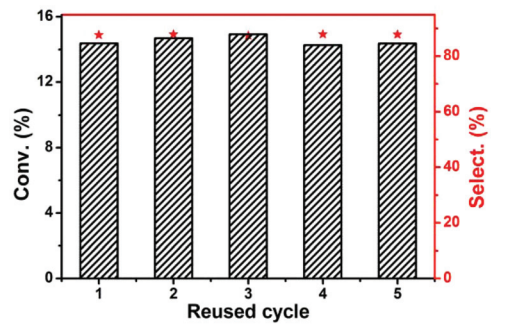

Fig. 11 A typical conversion and selectivity course of cyclohexane production with Au-in-CNTs as photocatalysts under Xe lamp irradiation. The catalyst was reused for 5 times.

Conclusions

In summary, Au nanoparticles confined in carbon nanotubes (Au-in-CNTs) are prepared successfully. Structural characterization by various techniques reveals that the Au nanoparticles are trapped into the short CNTs. The prepared catalyst, Au-in-CNTs, is active for the oxidation of cyclohexane with 14.64% conversion of cyclohexane and a high selectivity of 86.88% of cyclohexanol under quite mild conditions (333 K, in air, 48 h, with a Xe lamp, TBHP using as the initiating agent). The catalyst is environmentally friendly. Au-in-CNTs decrease the amount of noble metals and enhance the catalyst effect. Moreover, the catalyst is stable in the reaction system with excellent repeatability. This synergetic confinement effect of metal nanoparticles inside CNTs can lead to new advances and applications pertaining to functional materials in electronic, magnetic and catalytic fields, and related processes.

Acknowledgements

This work was supported by the National Basic Research Program of China (973 Program) (2012CB825803, 2013CB932702), the National Natural Science Foundation of China (51132006), the Specialized Research Fund for the Doctoral Program of Higher Education (20123201110018), a Suzhou Planning Project of Science and Technology (ZXG2012028), and a project funded by the Priority Academic Program Development of Jiangsu Higher Education Institutions.

Notes and references

1 G. Li, M. Xu, S. C. Larsen and V. H. Grassian, *J. Mol. Catal. A: Chem.*, 2003, **194**, 169.
2 M. T. Musser, in *Encyclocarbons of Industrial Chemistry*, ed. W. Gerhartz, Wiley, VCH, Weinheim, 1987, p. 217.
3 C. Nguyen, R. J. Guajardo and P. K. Mascharak, *Inorg. Chem.*, 1996, **35**, 6273.
4 P. Comba, M. Maurer and P. Vadivelu, *J. Phys. Chem. A*, 2008, **112**, 13028.
5 M. Dugal, G. Sankar, R. Raja and J. M. Thomas, *Angew. Chem., Int. Ed.*, 2000, **39**, 2310.
6 A. K. Suresh, M. M. Sharma and T. Sridhar, *Ind. Eng. Chem. Res.*, 2000, **39**, 3958.
7 J. L. Gu, Y. Huang, S. P. Elangovan, Y. S. Li, W. R. Zhao, I. Toshio, Y. Yamazaki and J. L. Shi, *J. Phys. Chem. C*, 2011, **115**, 21211.
8 N. Perkas, Y. Q. Wang, Y. Koltypin and A. Gedanken, *Chem. Commun.*, 2011, **11**, 988.

9 J. Li, Y. Shi, L. Xu and G. Z. Lu, *Ind. Eng. Chem. Res.*, 2010, **49**, 5392.
10 M. Alvaro, B. Cojocaru, A. A. Ismail, N. Petrea, B. Ferrer, F. A. Harraz, V. I. Parvulescu and H. Garcia, *Appl. Catal., B*, 2010, **99**, 191.
11 P. Falaras, I. M. Arabatzis, T. Stergiopoulos and M. C. Bernard, *Int. J. Photoenergy*, 2003, **5**, 123.
12 J. Y. Lan, X. M. Zhou, G. Liu, J. G. Yu, J. C. Zhang, L. J. Zhi and G. J. Nie, *Nanoscale*, 2011, **3**, 5161.
13 L. P. Wen, B. S. Liu, C. Liu and X. J. Zhao, *J. Wuhan Univ. Technol., Mater. Sci. Ed.*, 2009, **24**, 258.
14 M. M. Mohamed and K. S. Khairou, *Microporous Mesoporous Mater.*, 2011, **142**, 130.
15 A. Primo, A. Corma and H. Garcia, *Phys. Chem. Chem. Phys.*, 2011, **13**, 886.
16 R. H. Liu, H. Huang, H. T. Li, Y. Liu, J. Zhong, Y. Y. Li, S. Zhang and Z. H. Kang, *ACS Catal.*, 2014, **4**, 328.
17 L. Langer, V. Bayot, E. Grivei, J.-P. Issi, J. P. Heremans, C. H. Olk, L. Stockman, C. Van Haesendonck and Y. Bruynseraede, *Phys. Rev. Lett.*, 1996, **76**, 479.
18 T. W. Ebbesen, H. J. Lezec, H. Hiura, J. W. Bennett, H. F. Ghaemi and T. Thio, *Nature*, 1996, **382**, 54.
19 P. G. Collins, M. Hersam, M. Arnold, R. Martel and P. Avouris, *Phys. Rev. Lett.*, 2001, **86**, 3128.
20 J. P. Lu, *Phys. Rev. Lett.*, 1997, **79**, 1297.
21 E. Hernández, C. Goze, P. Bernier and A. Rubio, *Phys. Rev. Lett.*, 1998, **80**, 4502.
22 H. Kataura, Y. Kumazawa, Y. Maniwa, I. Umezu, S. Suzuki, Y. Ohtsuka and Y. Achiba, *Synth. Met.*, 1999, **103**, 2555.
23 L. Zhang, X. Tu, K. Welsher, X. Wang, M. Zheng and H. Dai, *J. Am. Chem. Soc.*, 2009, **131**, 2454.
24 F. Hoxha, L. Königsmann, A. Vargas, D. Ferri, T. Mallat and A. Baiker, *J. Am. Chem. Soc.*, 2007, **129**, 10582.
25 T. Brgi and A. Baiker, *Acc. Chem. Res.*, 2004, **37**, 909.
26 E. Tálas, J. L. Margitfalvi and O. Egyed, *J. Catal.*, 2009, **266**, 191.
27 H. U. Blaser and M. Studer, *Acc. Chem. Res.*, 2007, **40**, 1348.
28 Z. J. Chen, Z. H. Guan, M. R. Li, Q. H. Yang and C. Li, *Angew. Chem., Int. Ed.*, 2011, **50**, 4913.
29 W. Chen, X. L. Pan and X. H. Bao, *J. Am. Chem. Soc.*, 2007, **129**, 7421.
30 L. Yu, W. X. Li, X. L. Pan and X. H. Bao, *J. Phys. Chem. C*, 2012, **116**, 16461.
31 J.-P. Tessonnier, L. Pesant, G. Ehret, M.-J. Ledoux and C. Pham-Huu, *Appl. Catal., A*, 2005, **288**, 203.
32 P. M. Ajayan, O. Stephan, Ph. Redlich and C. Colliex, *Nature*, 1995, **375**, 564.
33 C. Pham-Huu, N. Keller, C. Estournes, G. Ehret and M. J. Ledoux, *Chem. Commun.*, 2002, 1882.
34 S. Webster, J. Maultzsch, C. Thomsen, J. Liu, R. Czerw, M. Terrones, F. Adar, C. John, A. Whitley and D. L. Carroll, *Mater. Res. Soc. Symp. Proc.*, 2003, **772**, 7.8.1.
35 M. Mandal, N. R. Jana, S. Kundu, S. K. Ghosh, M. Panigrahi and T. Pal, *J. Nanopart. Res.*, 2004, **6**, 53.
36 A. Jorio, R. Saito, J. H. Hafner, C. M. Lieber, M. Hunter, T. McClure, G. Dresselhaus and M. S. Dresselhaus, *Phys. Rev. Lett.*, 2001, **86**, 1118.
37 F. Tulnstra and J. L. Koenig, *J. Chem. Phys.*, 1970, **53**, 1126.
38 L. Y. Zeng, W. B. Wang, J. Q. Liang, Z. Q. Wang, Y. X. Xia, D. Lei, X. G. Ren, N. Yao and B. L. Zhang, *Mater. Chem. Phys.*, 2008, **108**, 82.
39 R. B. Rakhi, X. Lim, X. Gao, Y. Wang, A. T. S. Wee, K. Sethupathi, S. Ramaprabhu and C. H. Sow, *Appl. Phys. A*, 2010, **98**, 195.
40 X. X. Yang, H. Yu, F. Peng and H. J. Wang, *ChemSusChem*, 2012, **7**, 1213.
41 T. Miyake, M. Hamada, Y. Sasaki and M. Oguri, *Appl. Catal., A*, 1995, **131**, 33.
42 M. S. El-Deab, T. Sotomura and T. Ohsaka, *Electrochem. Commun.*, 2005, **7**, 29.
43 W. Chen, Z. L. Fan, X. L. Pan and X. H. Bao, *J. Am. Chem. Soc.*, 2008, **130**, 9414.